sustainability

MDPI

Article

Low-Emissivity Cavity Treatment for Enhancing Thermal Performance of Existing Window Frames

Maohua Xiong [1,2,3,*], Jihoon Kweon [1,*] and Soobong Kim [1]

[1] Department of Architecture, Keimyung University, Daegu 42601, Republic of Korea
[2] College of Architecture and Design, Jiangxi University of Science and Technology, Ganzhou 341000, China
[3] China Construction Eighth Engineering Division Corp., Ltd., South China Branch, Guangzhou 510000, China
* Correspondence: xmh202309@163.com (M.X.); jkweon@kmu.ac.kr (J.K.); Tel.: +86-13632776339 (M.X.)

Abstract

Windows contribute 40–50% of envelope heat loss despite occupying only 1/8–1/6 of the surface area. Conventional frame retrofits rely on geometry optimization or cavity insulation yet remain limited by cost and invasiveness. This study introduces electrochemical polishing to reduce cavity surface emissivity of multi-cavity broken-bridge aluminum window frames to suppress radiative heat transfer, offering a non-invasive, low-cost retrofit strategy for existing building windows. Using a typical 75-series casement window, finite element analysis (MQMC) reveals that reducing cavity surface emissivity from 0.9 to 0.05 lowers frame U-values by 12.39–30.38% and whole-window U-values by 2.72–9.69%, with full-cavity treatment outperforming insulating-cavity-only by an average of 0.29 W/(m^2·K). EnergyPlus simulations across multiple climate zones show 0.74–2.26% annual heating and cooling energy savings (with max reduction of 8.99 MJ/m^2·yr) in severe cold and cold regions (e.g., Harbin, Beijing), but 1.25–3.04% penalties in mild and hot-summer zones due to impeded nighttime heat rejection. At an incremental cost of 62.5 CNY/window (6.6–7.4% increase), the static payback period is 4.1 years in Harbin. The approach mitigates thermal bridging more effectively than foam-filled frames in whole-window performance. This scalable, minimal-intervention technology aligns with low-carbon retrofit imperatives for existing aging windows, particularly in heating-dominated climates.

Keywords: existing window retrofit; thermal performance; low-emissivity treatment; techno-economic analysis; computer simulation

1. Introduction

The building sector accounts for 29% of global final energy consumption and contributes approximately 40% of energy-related greenhouse gas (GHG) emissions [1]. With ongoing urbanization and population growth, energy demand in buildings is projected to increase, amplifying environmental and climatic impacts. In the context of urban renewal, retrofitting the vast stock of existing buildings is critical for enhancing occupant comfort, reducing operational energy use, and achieving carbon mitigation targets [2]. Consequently, building energy efficiency and decarbonization have emerged as policy priorities worldwide, including in China, where ambitious national strategies aim to peak carbon emissions before 2030 and attain neutrality by 2060.

As a critical component of the building envelope, windows mediate the exchange of heat, solar radiation, sound, air, vapor, and pollutants between indoor and outdoor environments, profoundly influencing both energy efficiency and indoor environmental

Check for updates

Academic Editors: Jiaqiang Wang and Linfeng Zhang

Received: 30 November 2025
Revised: 24 December 2025
Accepted: 30 December 2025
Published: 5 January 2026

Copyright: © 2026 by the authors. Licensee MDPI, Basel, Switzerland. This article is an open access article distributed under the terms and conditions of the Creative Commons Attribution (CC BY) license.

quality [3]. Although windows typically comprise only 1/8 to 1/6 of the envelope surface area, air infiltration and conductive/convective heat transfer through them account for 40–50% of total envelope heat loss in typical buildings [4]. Thus, enhancing window thermal performance is pivotal to elevating overall envelope energy efficiency.

In China, approximately 70 billion m^2 of existing buildings have accumulated over the past four decades [5]. Assuming a conservative window-to-wall ratio of 20%, the national window area exceeds 14 billion m^2 [6,7]. This immense stock suffers from performance degradation due to aging, material fatigue, and outdated thermal standards. Full-scale window replacement, while effective, incurs prohibitive costs and substantial embodied carbon emissions. Minor, targeted retrofitting—focusing on glazing upgrades or frame enhancements—has thus emerged as the dominant strategy for energy-efficient renovation.

The thermal performance of a window system is jointly governed by the glazing and frame. Significant advances in energy-efficient glazing—such as low-emissivity coated glass [8], functional films [9], insulating glass units [10], and thermochromic systems [11]—have substantially improved solar control and insulation. For instance, Chang [12] demonstrated that coated glass reduces inner-surface temperature by up to 10 °C under solar irradiation compared to ordinary glass, owing to superior infrared reflectance. Concurrently, frame optimization strategies—including geometric reconfiguration [13], material substitution [14,15], and advanced extrusion techniques [16]—have been explored. For example, Zajas [13] conducted a sensitivity analysis identifying key geometric parameters, achieving a minimum frame U-value of 0.71 $W/(m^2 \cdot K)$ through optimized cross-sectional design.

In typical existing broken-bridge aluminum windows, the frame accounts for 30–50% of the total heat loss through the window assembly, despite occupying only 20–30% of the area [3,4]. For a standard 6 + 12A + 6 Low-E glazing system (U_glazing ≈ 1.96 $W/(m^2 \cdot K)$), the frame U-value often exceeds 2.3 $W/(m^2 \cdot K)$, creating a significant thermal bridge at the frame–glazing interface. Reducing frame heat loss is therefore critical for improving overall window performance.

While conventional approaches primarily reduce thermal conductivity via material or geometric modifications, suppressing internal cavity heat transfer represents an emerging, complementary pathway—particularly suited to retrofitting. Low-cost interventions such as cavity filling, surface polishing, or film application can upgrade underperforming frames to meet current energy standards without structural alteration. This is especially relevant amid global decarbonization imperatives [17]. Cavity insulation has been widely investigated: Paulos [18] reported 4–29% frame U-value reductions via aerogel filling across 48 commercial profiles, with full-cavity implementation yielding up to 35% improvement. Similarly, Agnieszka [19] achieved a ~27% reduction in PVC frame U-value through polyurethane foam injection, without altering geometry or base material. An alternative, underexplored approach involves modifying cavity inner-surface emissivity. Per fundamental heat transfer principles, lowering surface emissivity suppresses radiative exchange, thereby reducing overall cavity heat flux. Although widely applied in glazing (e.g., Low-E coatings), this strategy has seen limited adoption in frames, with prior studies offering only preliminary insights [19].

Common frame retrofit strategies include increasing profile thickness, adding polyurethane foam filling, or replacing with high-performance materials (e.g., wood, PVC-U). While these methods can reduce frame U-values, they often involve significant structural modifications, increased material costs, and potential aesthetic or installation constraints. Moreover, foam filling achieves diminishing returns beyond U_frame ≈ 1.5 $W/(m^2 \cdot K)$, and thicker profiles may not be feasible in existing window openings. In contrast, modifying the inner-surface emissivity of multi-cavity aluminum frames offers a non-intrusive, low-cost alternative that targets radiative heat

transfer—the dominant mechanism in sealed cavities—without altering frame geometry or requiring replacement.

Addressing this gap, the present work systematically evaluates low-emissivity treatment—via electrochemical polishing—on the inner surfaces of multi-cavity broken-bridge aluminum frames. Using a typical 75-series casement window as the baseline, finite element analysis (MQMC) quantifies U-value improvements, while EnergyPlus modeling across five Chinese climate zones elucidates regional energy-saving potential and applicability. This non-invasive, low-cost retrofit pathway offers significant promise for advancing near-zero energy and carbon-neutral building goals through scalable, minimal-intervention upgrades to the nation's aging window stock. The flowchart of this study is illustrated in Figure 1.

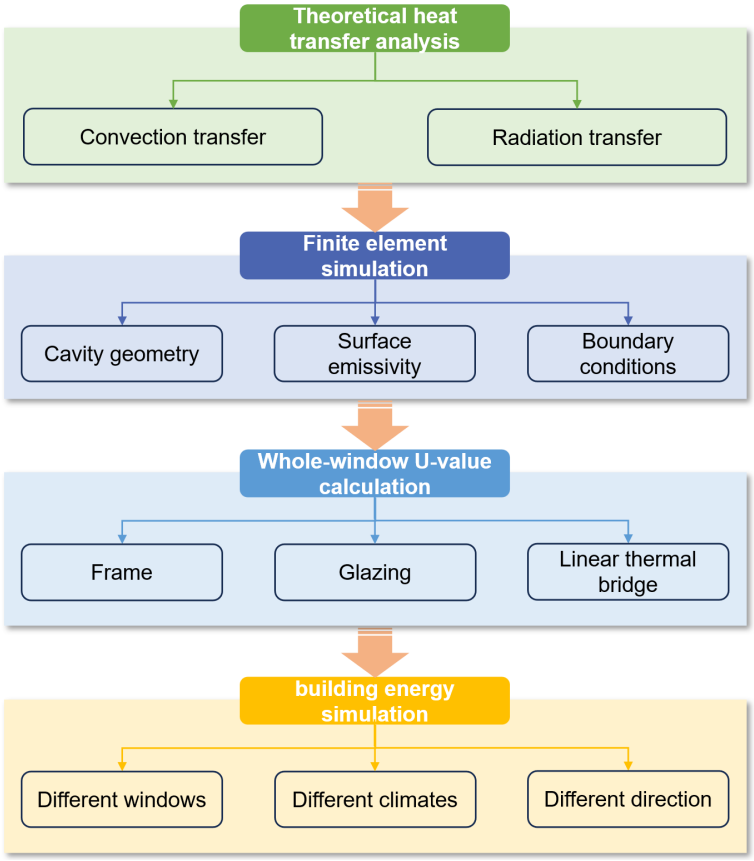


Figure 1. Flowchart of this study.

2. Methods

2.1. Window's Thermal Performance Calculation Method

2.1.1. Analysis of Heat Transfer in the Cavity

Heat transfer within the cavity occurs via natural convection and radiation, and is governed by several key factors: cavity geometry, orientation (vertical, horizontal, or inclined), surface emissivity, and thermophysical properties of the enclosed gas. To streamline the analysis, the concept of equivalent thermal conductivity (λ_{eq}) is adopted. As defined in EN ISO 10077-2 [20], λ_{eq} is expressed as in Equation (1):

$$\lambda_{eq} = \frac{d}{R_s} \quad (1)$$

where, as illustrated in Figure 2a, d denotes the cavity depth (m), b is the dimension perpendicular to the depth direction (m), and R_s represents the equivalent thermal resistance ($m^2 \cdot K/W$), which can be calculated as follows:

$$R_s = \frac{1}{h_a + h_r} \tag{2}$$

where h_a is the combined conductive–convective heat transfer coefficient ($W/m^2 \cdot K$), and h_r is the radiation heat transfer coefficient ($W/m^2 \cdot K$).

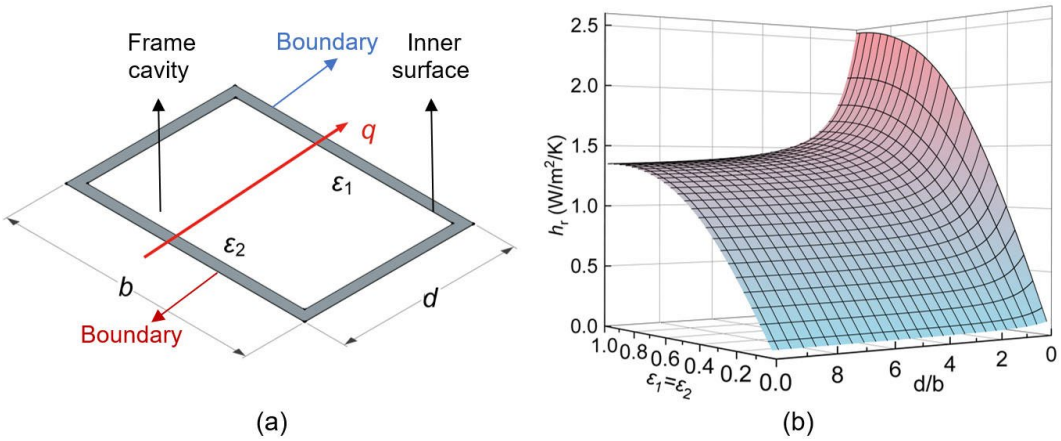


Figure 2. (**a**) Section diagram of cavity and its heat transfer, (**b**) relationship of radiation heat transfer coefficient with cavity inner surface emissivity and cavity geometry [21].

Thus, the core of the heat transfer analysis lies in determining the dominant factors influencing h_a and h_r through their definitions and governing expressions.

The convective heat transfer coefficient h_a describes the heat transfer through heat conduction and convection in the cavity, and is computed as following Equation (3).

$$h_a = \max\left\{\frac{C_1}{d}; C_2 \Delta T^{1/3}\right\} \tag{3}$$

where $C_1 = 0.025$ W/(m·K), $C_2 = 0.73$ W/($m^2 \cdot K^{4/3}$).

The maximum value in Equation (3) is governed by the cavity depth d and the temperature difference ΔT across the inner surfaces. At small depths (d = 13–15 mm), heat transfer is conduction-dominated, with negligible influence from surface temperature. As d increases, heat transfer becomes ΔT-dependent, transitioning primarily to convective mode.

The radiation heat transfer coefficient is calculated as in Equation (4).

$$h_r = 4\sigma T_m^3 EF \tag{4}$$

where σ is the Stephen-Boltzmann constant, 5.67×10^{-8} W/($m^2 \cdot K^4$); T_m is the average cavity temperature (reference value 283 K); E is the system emissivity, $E = ((1/\varepsilon_1) + (1/\varepsilon_2) - 1)^{-1}$, and ε_1, ε_2 represent the emissivity of surface 1 and surface 2, respectively; F is the view factor for the rectangular cross-section, which can be derived from Equation (5).

$$F = 1/2 \times (1 + \sqrt{1 + (d/b)^2} - (d/b)) \tag{5}$$

As shown in Equation (4), h_r depends on three independent parameters: T_m, E, and F. Given that the mean cavity temperature T_m varies only slightly from the reference value of 283 K across the studied cases, its influence on h_r is negligible. The parameters E and F encapsulate the surface emissivity (ε_1, ε_2) and cavity geometry (aspect ratio d/b),

respectively. Radiation heat transfer within the cavity is strongly governed by the emissivity of the internal surfaces. As surface emissivity increases, the effect of the view factor becomes more pronounced. Moreover, at lower aspect ratios (d/b), h_r exhibits greater sensitivity to ε (Figure 2b), indicating that the emissivity of surfaces perpendicular to the heat flow direction exerts a dominant influence on radiative transfer intensity. For brevity, results for varying surface emissivity combinations are omitted, but follow a similar trend to Figure 2b: even a single low-emissivity surface substantially reduces cavity heat transfer.

2.1.2. Simulation Methodology

There are two primary approaches for investigating window thermal performance: experimental testing and computer simulation. Compared to experimental methods, computer simulations offer substantial savings in manpower and material costs while maintaining computational accuracy [18,22]. MQMC is an indigenous Chinese software for window thermal performance calculations, integrating functionalities from Optics, Therm, and Window—tools originally developed by Lawrence Berkeley National Laboratory [23]. It encompasses optical–thermal performance analysis for glazing systems, two-dimensional finite element heat transfer modeling for window frames, and overall window thermal performance evaluation. Accordingly, this study employs MQMC to compute the thermal transmittance of window frames and entire assemblies following modifications to the inner surface emissivity of various cavities, adhering to established modeling protocols to validate simulation reliability [18,24].

Mesh independence was verified using window frame 1 in Case B (see Table 1) as a test case. Four maximum element sizes (3, 4, 5, and 6 mm) were examined, yielding a maximum relative difference in frame U-value of less than 0.1% relative to the finest mesh. A maximum element size of 4 mm was adopted for all simulations, ensuring numerical accuracy while maintaining reasonable computational time.

Table 1. Window frame simulation scenarios setting.

Scenario	Cavity Type	Inner Surface Emissivity	Note
A	Polyurethane foam filling	—	Filling only the insulation cavity
B	Ordinary surface	0.9	Reference case
C-1	Low-emissivity surface	0.2	All cavity interior surfaces are treated
D-1	Ultra-low-emissivity surface	0.05	
C-2	Low-emissivity surface	0.2	Insulation cavity treatment only
D-2	Ultra-low-emissivity surface	0.05	

2.1.3. Description of the Window Frame

To ensure the representativeness of simulation results, a typical 75-series broken-bridge aluminum alloy casement window is selected as the research object. In accordance with Chinese standards for window specifications and dimensions [25,26], a 600 × 1200 mm single-sash broken-bridge aluminum alloy casement window is adopted as the simulation model (Figure 3a). The aluminum alloy frame comprises four frames. Since vertical frames 3 and 4 are symmetrically embedded against the wall and exhibit identical heat transfer behavior, only the thermal transmittance at node 3 is calculated to reduce computational cost.

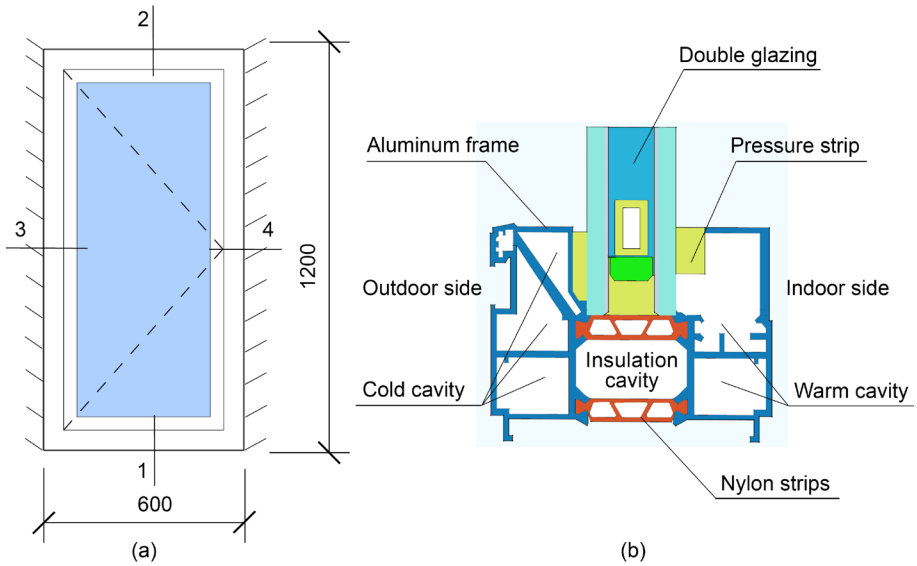


Figure 3. Sectional view of the (**a**) facade and (**b**) frame of the broken bridge aluminum alloy window.

All frame profiles share an identical multi-cavity structure, consisting of three cold cavities, one insulating cavity, and two warm cavities (Figure 3b). The glazing system is configured as 6 + 12A + 6 Low-E glass, with a thermal transmittance of 1.96 W/(m^2·K), visible light transmittance of 0.51, and shading coefficient of 0.53.

2.1.4. Scenario Setting

The surface emissivity of a material is primarily governed by its surface properties. Accordingly, three inner-surface emissivity scenarios (Cases B, C, and D) were designed based on the aluminum alloy surface characteristics listed in Table 1. To benchmark the thermal performance of low-emissivity versus filled window frames, the original broken-bridge aluminum alloy frame configuration is included as Case A, where only the insulating cavity is filled with polyurethane foam [27]. Case B represents a conventional colored aluminum alloy surface and serves as the reference. Case C simulates a low-emissivity surface, corresponding to the cavity inner surface after oxidation and polishing. Case D models an ultra-low-emissivity surface, representing the cavity interior following film deposition or coating. The numeric suffix 1 in Cases C and D denotes low-emissivity treatment applied to all cavity surfaces, whereas suffix 2 indicates treatment limited to the insulating cavity inner surface. It should be noted that the ultra-low emissivity value of $\varepsilon = 0.05$ for Case D is based on literature for highly polished aluminum surfaces [28–31]. While electrochemical polishing can consistently achieve $\varepsilon < 0.08$ in complex geometries, attaining exactly 0.05 uniformly across all cavity surfaces may require optimized process parameters.

2.1.5. Boundary Conditions

The boundary conditions applied in the simulations are detailed in Table 2, in compliance with Chinese standards for window thermal performance calculations [32]. Specifically, when determining the thermal transmittance of doors and windows, the outdoor convective heat transfer coefficient $h_{c,out}$ is set to 8 W/(m^2·K) for the frame perimeter and 12 W/(m^2·K) for the glazing edge within 65 mm of the frame. Additionally, the shading coefficient and total solar transmittance are calculated using standard summer design conditions. The absence of solar radiation in the winter conditions follows the requirements of GB/T 8484-2020 [33] and JGJ/T 151-2008 [32], which mandate zero solar irradiation for steady-state thermal transmittance determination to isolate temperature-driven heat transfer.

Table 2. Thermal simulation boundary conditions.

Boundary Conditions	Winter Boundary Conditions	Summer Boundary Conditions
Indoor air temperature T_{in}	20 °C	25 °C
Outdoor air temperature T_{out}	−20 °C	30 °C
Indoor convective heat transfer coefficient $h_{c,in}$	3.6 W/(m^2·K)	2.5 W/(m^2·K)
Outdoor convective heat transfer coefficient $h_{c,out}$	16 W/(m^2·K)	16 W/(m^2·K)
Indoor average radiant temperature $T_{rm,in}$	20 °C	25 °C
Outdoor average radiant temperature $T_{rm,out}$	−20 °C	30 °C
Solar irradiance I_s	0 W/m^2	500 W/m^2

2.2. Energy Consumption Simulation Method

Using the calculated thermal performance of doors and windows, EnergyPlus is employed to evaluate the impact of the broken-bridge aluminum alloy casement window, incorporating various frame types, on the annual heating and cooling energy consumption of a typical office room across different thermal climate zones in China. The approach of analyzing energy-saving effects with a single room as the study object is well-established in the literature [34,35]. As depicted in Figure 4, the room dimensions are 5.00 × 4.00 × 3.00 m (length × width × height), with six external windows, each measuring 0.60 × 1.20 mm, resulting in a window-to-wall area ratio of 0.36.

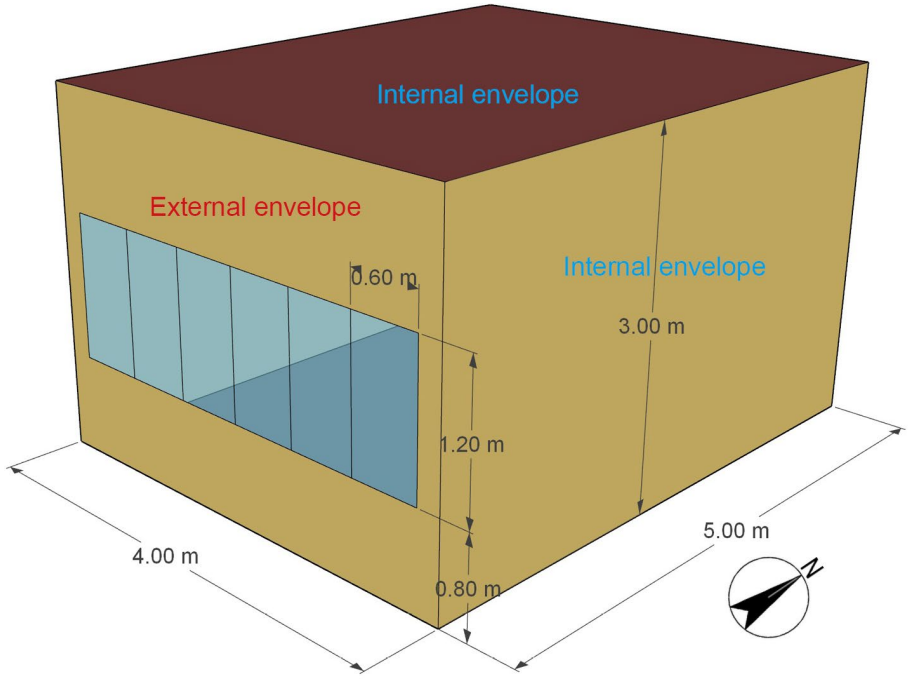


Figure 4. Schematic diagram of the simulated room.

To isolate the influence of other building envelopes and emphasize the impact of varying external window performance, a single-zone office room model is employed, with one external wall containing six windows and the remaining walls, floor, and ceiling designated as internal (adiabatic) envelopes (Figure 4). This simplification, widely adopted in prior window retrofit studies to highlight relative performance differences [34,35], is extended here to enhance representativeness by considering multiple window orientations.

Additional EnergyPlus simulations are conducted with the external wall and windows facing north, east, west, and south. For each climate zone and window configuration (Cases A to D-2), annual heating and cooling energy consumption is calculated separately for the four cardinal orientations. The reported results represent the orientation-averaged

values, while orientation-specific data are provided in Table A1 for completeness. This multi-orientation averaging mitigates bias from high solar gains on south façades and improves the generalizability of findings to typical multi-façade buildings [36].

The thermal transmittance of the external wall in different thermal climate zones is specified in Table 3, adhering to the Public Building Energy Efficiency Design Standard (GB 50189-2015) [37]. As for the thermal transmittance of the external window (Cases A to D-2), it is determined based on calculations in Section 2.2. All external windows have a solar heat gain coefficient (SHGC) of 0.34 and a visible light transmittance of 37%. Notably, in cold and severe cold regions, the thermal transmittance of the external window does not comply with energy-efficient design standards. However, as the analysis focuses on comparing energy-saving rates within the same region using different window configurations, rather than inter-regional energy consumption, the simulation results remain valid for identifying performance trends.

Table 3. Thermal transmittance of external wall in different thermal climate zones.

Thermal Climate Zone	Typical Cities	U (W/(m^2·K))
Severe cold	Harbin	0.35
Cold	Beijing	0.45
Hot summer and cold winter	Shanghai	0.8
Hot summer and warm winter	Guangzhou	1.5
Temperate	Kunming	1.5

The occupancy density, lighting load, appliance load, and fresh air supply, along with their schedules, were configured in accordance with GB 50189-2015 [37]. On weekdays from 06:00 to 19:00, the indoor air temperature is maintained at heating and cooling set-points of 22 °C and 26 °C, respectively. Additionally, heating and cooling setback temperatures are set to 5 °C and 37 °C, respectively, to prevent excessive indoor air temperatures during unoccupied periods in winter and summer.

Table 4 lists the representative cities for the five climate zones, with corresponding hourly average meteorological data—including ambient dry-bulb temperature, relative humidity, wind speed and direction, horizontal solar radiation, and cloud cover factor—imported as simulation boundary conditions. These data, formatted as Typical Meteorological Year (TMY) based on measured meteorological parameters [38], are compatible with building energy simulations in EnergyPlus.

Table 4. Meteorological conditions of the typical cities.

Typical Cities	Air Temperature (°C)	Relative Humidity (%)	Wind Speed (m/s)	Horizontal Solar Radiation (Wh/m^2)
Harbin	4.1	66.2	3.1	145.5
Beijing	12.6	55.4	2.4	159.9
Shanghai	16.7	76.0	3.2	145.1
Guangzhou	22.2	76.9	1.7	129.7
Kunming	15.5	70.1	1.4	174.7

2.3. Techno-Economic Analysis

The techno-economic viability of the low-emissivity cavity inner-surface treatment, achieved through electrochemical polishing, is assessed via incremental cost estimation and life-cycle cost–benefit analysis for the simulated office room (5000 × 4000 × 3000 mm, six 600 × 1200 mm south-facing windows, WWR = 0.36).

The frame perimeter per window (P_f) is calculated as in Equation (6).

$$P_f = 2 \times (w + h) = 2 \times (0.6 + 1.2) = 3.6\ m \quad (6)$$

where w and h are the window width and height, respectively, which can be derived from Figure 3a.

The treatment area (A_{full}) for full-cavity application is determined as in Equation (7).

$$A_{full} = P_f \times L_c = 3.6 \times 0.28 = 1.008\ m^2 \quad (7)$$

where L_c is the inner surface perimeter of all cavities, which can be measured from Figure 3b.

The incremental cost per window (C_{inc}) is computed as in Equation (8).

$$C_{inc} = A \times c_p \quad (8)$$

where c_p (CNY/m^2) is the unit polishing cost, industry range is 45–80 CNY/m^2 [39,40], with an average of 62 CNY/m^2. The total initial investment for the room is $C_{total} = 6 \times C_{inc}$.

Annual energy savings (ΔE, kWh/yr) are derived from EnergyPlus simulations, converted from MJ/m^2·yr to kWh/m^2·yr using 1 kWh = 3.6 MJ, and scaled to the room floor area ($A_f = 20$ m^2):

$$\Delta E = \Delta e \times A_f \quad (9)$$

where Δe is the specific saving (kWh/m^2·yr) relative to Case B (see Section 3.2).

Annual monetary savings (S) are calculated as follows:

$$S = \Delta E \times r_e \quad (10)$$

where $r_e = 0.85$ CNY/kWh is the commercial electricity tariff. This assumes electrically driven systems for both heating and cooling; in reality, district heating prevails in northern severe cold and cold zones, potentially yielding higher effective savings due to lower heating energy costs.

The static payback period (SPP) is given by:

$$\mathrm{SPP} = \frac{C_{total}}{S} \quad (11)$$

The economic analysis considers only the initial incremental cost of electrochemical polishing and annual energy savings based on electricity tariffs. Maintenance costs (e.g., periodic cleaning or potential surface re-treatment) and life-cycle considerations (e.g., durability of the polished surface over 20 years) were not included due to the lack of long-term empirical data. However, electrochemical polishing is a durable industrial process with minimal maintenance requirements, and the treated surfaces are expected to remain stable under normal indoor conditions. A full life-cycle cost analysis (LCCA) incorporating maintenance, potential replacement, and end-of-life recycling will be addressed in future studies.

3. Results

3.1. Thermal Performance Comparison

3.1.1. Thermal Transmittance of Window Frame

Figure 5a presents the temperature field distributions for window frame 1 under Cases A, B, C-1, and D-1. The temperature contours for Cases C-2 and D-2 (treatment limited to the insulating cavity only) are qualitatively similar to those of Cases C-1 and

D-1, respectively, with only minor differences in absolute temperature values due to the smaller overall emissivity reduction. Under identical boundary conditions, Case A exhibits the highest indoor-side temperature, indicating the best thermal insulation performance. Conversely, Case B shows the lowest indoor-side temperature, reflecting the poorest insulation. Comparison of the temperature contours for Cases B, C-1, and D-1 reveals that as inner-surface emissivity decreases, the indoor-side temperature progressively increases, thereby enhancing the insulation effect.

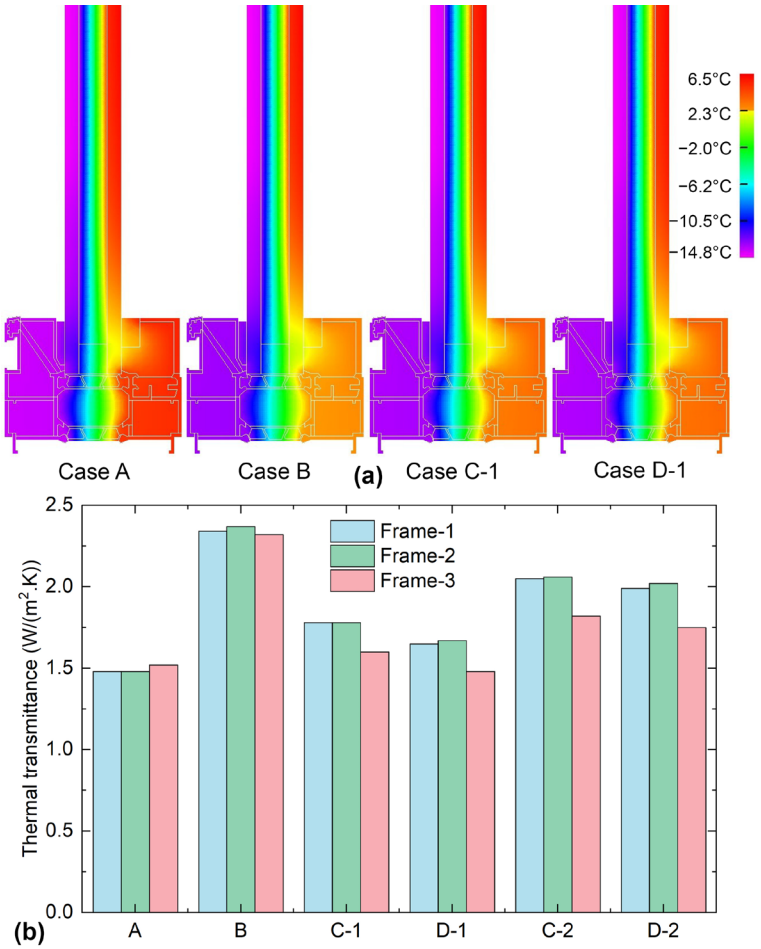


Figure 5. Thermal performance of window frames under different scenarios, (**a**) temperature field distribution of window frame 1 under four scenarios, (**b**) thermal transmittance of window frames under different scenarios.

Furthermore, as shown in Figure 5b, the Case B frame with a conventional surface exhibits the highest thermal transmittance, ranging from 2.32 to 2.37 W/(m^2·K). As cavity inner-surface emissivity decreases, the thermal transmittance of the broken-bridge aluminum alloy frame diminishes correspondingly, achieving reductions of 12.39–30.38% relative to the baseline (Cases C-1 to D-2). This improvement stems from suppressed radiative heat transfer within the cavities, which reduces overall heat flux and frame thermal transmittance. A detailed mechanistic analysis is presented in Section 2.1.1.

Moreover, the thermal transmittance of low-emissivity frames varies substantially depending on the scope of surface treatment. As illustrated in Figure 5b, applying low-emissivity coating to all cavity surfaces yields a thermal transmittance of 1.48–1.78 W/(m^2·K). In contrast, treatment limited to the insulating cavity results in 1.75–2.06 W/(m^2·K), with an average difference of 0.29 W/(m^2·K) between the two strate-

gies. Therefore, comprehensive low-emissivity treatment across all cavity surfaces maximizes the thermal insulation performance of the window frame.

Given the nascent application of low-emissivity treatments for enhancing window frame thermal performance, a comparative assessment against conventional filled frames is essential to evaluate their engineering viability and adoption potential. As shown in Figure 5b, the ultra-low-emissivity treatment applied to all cavity surfaces (Case D-1) results in an average thermal transmittance only 0.10 W/(m^2·K) higher than the polyurethane foam-filled frame (Case A). Although the low-emissivity frame does not fully match the insulation performance of the filled frame, the relative difference is merely 6.70%. additionally, the cost of coating is lower than that of filling insulation materials.

Furthermore, low-emissivity treatment can be synergistically combined with filled frames by applying it to the inner surfaces of cold and warm cavities, while retaining polyurethane foam in the insulating cavity. Simulation results demonstrate that this hybrid strategy reduces thermal transmittance by approximately 0.25 W/(m^2·K), yielding a 16.90% improvement in thermal performance. Achieving equivalent enhancement through increased frame thickness alone would require expanding the broken-bridge aluminum alloy profile from 75 mm to 85 mm. Thus, it can be expected that low-emissivity treatment provides a cost-effective approach to further optimize the thermal performance of existing filled window frames.

3.1.2. Thermal Transmittance of Whole Window

Although the thermal performance of individual window frames varies significantly, the overall window thermal transmittance exhibits more modest differences. For the standard inner-surface configuration (Case B), the broken-bridge aluminum alloy window achieves the highest thermal transmittance of 2.75 W/(m^2·K). Consistent with frame-level trends, lower cavity inner-surface emissivity correlates with reduced whole-window thermal transmittance. Relative to Case B, low-emissivity treatments yield reductions of 0.08–0.27 W/(m^2·K), corresponding to improvements of 2.72–9.69% (Figure 6).

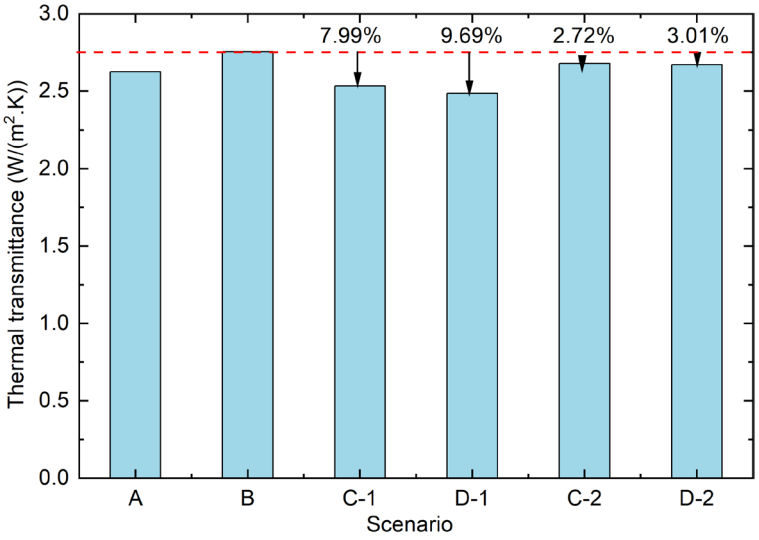


Figure 6. Thermal transmittance of whole window under different scenarios.

However, comparison of Figures 5 and 6 reveals that the whole-window thermal transmittance of the polyurethane foam-filled frame (Case A) exceeds that of Cases C-1 and D-1. This counterintuitive result arises from the substantial disparity between the thermal transmittance of the filled frame and the 6 + 12A + 6 Low-E glazing system, which amplifies the thermal bridge effect at the frame–glazing junction. As shown in

Table 5, the linear thermal transmittance (ψ) at this interface is higher for the filled frame (0.18 W/(m·K)) than for the low-emissivity frames (approximate 0.15 W/(m·K)). Therefore, the thermal transmittance of the glazing system and window frame must be appropriately matched to minimize thermal bridging and linear thermal transmittance at their interface. A lower frame thermal transmittance does not necessarily guarantee superior overall window performance.

Table 5. Thermal transmittance and linear thermal transmittance of window frames under scenarios of A, C-1 and D-1.

Scenario	Cavity Type	Frame Number	Thermal Transmittance (W/(m^2·K))	Linear Thermal Transmittance (W/(m·K))
A	Polyurethane foam filling	1	1.48	0.18
		2	1.48	0.18
		3	1.52	0.18
C-1	Low-emissivity surface	1	1.78	0.15
		2	1.78	0.15
		3	1.60	0.15
D-1	Ultra-low-emissivity surface	1	1.65	0.14
		2	1.67	0.14
		3	1.48	0.15

3.2. Building Energy Saving Effect

As shown in Figure 7, the impact of cavity inner-surface low-emissivity treatment varies significantly across climate zones. In Harbin (severe cold zone), energy consumption decreases monotonically with reduced window thermal transmittance, with Case D-1 achieving the lowest value of 387.79 MJ/m^2·yr, representing a 2.26% reduction compared to Case B (396.78 MJ/m^2·yr). Case C-1 follows at 389.39 MJ/m^2·yr (−1.86%), while cases with treatment confined to the insulating cavity (C-2 and D-2) yield 394.05–394.32 MJ/m^2·yr, underscoring the importance of full-cavity treatment in heating-dominated climates. A similar trend emerges in Beijing (cold zone), where Case D-1 registers 223.70 MJ/m^2·yr, a 0.74% reduction over Case B (225.36 MJ/m^2·yr), confirming consistent but moderate energy savings.

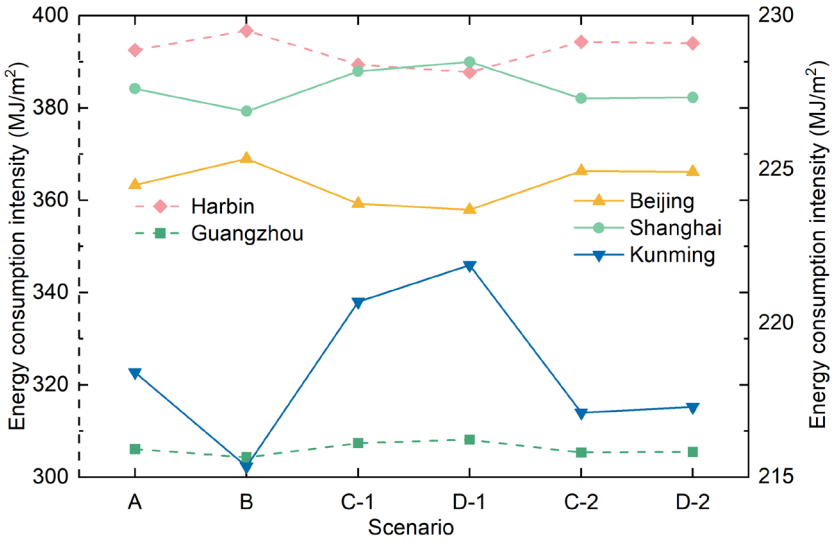


Figure 7. The annual energy consumption of heating and air conditioning per unit area of office room under different simulation scenarios.

In Shanghai (hot summer, cold winter zone), energy consumption remains largely insensitive to frame treatment, ranging narrowly from 226.90 MJ/m^2·yr (Case B) to 228.50 MJ/m^2·yr (Case D-1), reflecting the offsetting effects of reduced winter heat loss and impaired summer heat rejection. In contrast, in Guangzhou (hot summer, warm winter) and Kunming (mild climate), energy use increases slightly with decreasing window thermal transmittance. In Guangzhou, Case D-1 reaches 308.11 MJ/m^2·yr, a 1.25% increase over Case B (304.30 MJ/m^2·yr); in Kunming, Case D-1 is 221.90 MJ/m^2·yr, 3.04% higher than Case B (215.35 MJ/m^2·yr).

Overall, full-cavity low-emissivity treatment (Cases C-1 and D-1) delivers 0.7–2.3% energy savings in severe cold and cold regions (Harbin and Beijing), exhibits near-neutral performance in transitional climates (Shanghai), and incurs minor penalties of 1.0–3.0% in cooling-influenced zones (Guangzhou and Kunming). The technology remains recommended primarily for climates with predominant heating demands, while its application in balanced or cooling-dominated regions requires careful consideration of façade orientation and solar exposure.

3.3. Techno-Economic Comparison

As shown in Figure 8a, a standard 75-series broken-bridge aluminum window with 6 + 12A + 6 Low-E glazing has a factory price of approximately 850–950 CNY. The low-emissivity treatment therefore increases the window cost by 6.6–7.4%, with full-cavity ultra-low-emissivity treatment (Case D-1) adding 62.5 CNY.

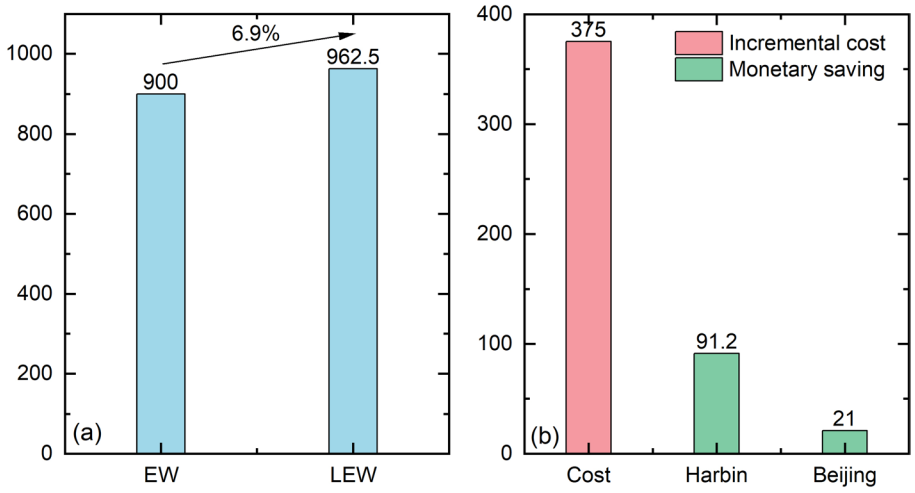


Figure 8. (**a**) comparison of cost between exist window (EW) and low-emissivity window (LEW), (**b**) incremental cost of six windows and maximum annual monetary savings in Harbin and Beijing.

For the simulated room, the six-window increment totals 375.0 CNY, and the maximum annual monetary savings are thus 91.2 CNY in Harbin and 21.0 CNY in Beijing (see Figure 8b), respectively. The static payback period for the 375.0 CNY investment is 4.1 years in Harbin and 17.9 years in Beijing.

In summary, full-cavity electrochemical polishing offers compelling economics in severe cold and cold climates, with payback below 5 years. In temperate and hot-summer regions, the technology should be limited to insulating-cavity treatment or avoided to prevent life-cycle cost penalties.

4. Discussion

4.1. Implications for Low-Carbon Window Retrofits

The proposed low-emissivity treatment of cavity inner surfaces markedly enhances the thermal performance of both window frames and complete assemblies, with frame U-values reduced by 12.39–30.38% and whole-window U-values by 2.72–9.69% relative to the baseline (Case B). These improvements are achieved at a modest incremental cost of 62.5 CNY per 600 × 1200 mm sash, representing only a 6.6–7.4% increase over the factory price of a standard 75-series broken-bridge aluminum window with 6 + 12A + 6 Low-E glazing. In Harbin (severe cold zone), the static payback period for full-cavity treatment is 4.1 years, driven by annual savings of 107 kWh per 20 m^2 office room. This aligns closely with the principles of minimal intervention and high cost-effectiveness advocated for existing building retrofits [41,42], offering a viable alternative to conventional frame thickening or foam filling, which typically require structural modifications.

4.2. Anisotropic Heat Transfer in Horizontal Versus Vertical Frames

An intriguing finding, illustrated in Figure 5, is the consistently lower U-value of vertical frames compared to horizontal frames in low-emissivity configurations, with the disparity widening as surface emissivity decreases. This anisotropy stems from two interrelated mechanisms. First, current two-dimensional finite element software for window thermal analysis, compliant with EN ISO 10077-2 [20], neglects buoyancy-driven convection in vertical sections due to the assumption of negligible gravitational effects perpendicular to the heat flow plane. In contrast, horizontal frames are modeled with gravity-aligned buoyancy, inducing stronger natural convection within cavities and elevating effective thermal conductivity. Second, as demonstrated in Section 2.1.1, lower surface emissivity suppresses radiative transfer, thereby increasing the relative contribution of convection to total heat flux. Consequently, the buoyancy-induced convective intensity in horizontal cavities is amplified at reduced emissivity, exacerbating the U-value differential. Therefore, it is necessary to develop three-dimensional conjugate heat transfer models and implement them into standards in the future, thus accurately capturing orientation-dependent performance, particularly for advanced low-emissivity frames where convection dominates.

4.3. Climate-Specific Energy-Saving Potential

The energy-saving efficacy of the low-emissivity treatment is highly climate-dependent, as evidenced by EnergyPlus simulations across five zones. In heating-dominated regions (Harbin, Beijing), full-cavity treatment (Case D-1) yields 2.5–3.0% reductions in annual heating and cooling energy use. However, in cooling-dominated or mild climates (Guangzhou, Kunming), the same treatment increases energy consumption by 1.2–3.2%, owing to restricted nighttime heat rejection through the south-facing façade under low U-value conditions. The Shanghai case exhibits near-neutral performance, reflecting balanced heating and cooling loads. These results highlight that low-emissivity frames are optimally suited to severe cold and cold zones, where heating degree-days exceed 3800, but risk cooling penalties in zones with high solar gain and moderate diurnal swings.

To extend applicability in transitional or cooling-dominated climates, hybrid strategies—such as applying low-emissivity treatment selectively to the insulating cavity only (Cases C-2/D-2) or combining it with switchable low-emissivity coatings that maintain higher emissivity during the cooling season—offer promising solutions. Alternatively, integrating the treatment with ventilated frame designs or external shading systems can preserve passive nighttime cooling while retaining winter benefits. Such tailored implementations warrant further investigation in future studies.

It should be noted that the reported cooling penalties in mild and hot-summer regions are derived from a simplified adiabatic single-room model excluding passive ventilation, night flushing, shading devices, and thermal mass effects. In real buildings, these strategies—particularly nighttime ventilation and external shading—can enhance heat rejection and potentially offset or reverse the adverse impacts of excessively low U-values. Consequently, the climate applicability of low-emissivity cavity treatment should be evaluated on a case-specific basis, incorporating building-specific operational patterns and envelope characteristics, rather than relying solely on generalized zonal recommendations.

4.4. Limitations and Future Study

Despite robust theoretical and numerical evidence, a primary limitation of the present study is the reliance on numerical simulations without accompanying experimental validation.

The assumed emissivity values ($\varepsilon \approx 0.8$–0.9 for standard surfaces, down to ≈ 0.05 for ultra-low-emissivity electrochemical polishing) are derived from literature and industry specifications; however, actual post-treatment emissivity may vary due to surface roughness, oxidation, and complex cavity geometries. Moreover, the long-term stability of polished surfaces under moisture exposure and thermal cycling has not been assessed. These uncertainties highlight the need for empirical confirmation.

Another consideration is the potential for emissivity gradients or local variations arising from uneven electrochemical polishing, surface contamination, or geometric constraints in deep cavities. While such heterogeneities could modestly elevate effective radiative transfer (particularly in partially treated cavities), their impact is expected to be secondary compared to the bulk emissivity reduction demonstrated here. Quantitative assessment via sensitivity analysis or high-resolution three-dimensional modeling, coupled with experimental emissivity mapping (e.g., infrared thermography), will be prioritized in future work to evaluate these effects and refine performance predictions.

Future research will focus on fabricating prototype frames with varying treatment levels and conducting hemispherical emissivity measurements (per ASTM E408 [43]) alongside hot-box testing (per GB/T 8484-2020 [33]) to validate U-value reductions and condensation resistance. Durability tests under accelerated aging protocols will also be performed to evaluate potential emissivity degradation over time.

The current methodology relies on steady-state finite element analysis (MQMC), consistent with international and Chinese standards for window thermal transmittance evaluation. While this approach provides robust comparative results, it does not capture transient effects or detailed three-dimensional flow patterns. Future work could extend the analysis using dynamic simulation tools such as TRNSYS for seasonal system performance or CFD-based models to resolve local convection and buoyancy-driven flows within cavities. Additionally, integrating the proposed low-emissivity frame treatment with advanced active systems—such as thermal diode tanks or solar-thermal-energy-storage-assisted heat pumps—may offer synergistic benefits for net-zero building retrofits, warranting further interdisciplinary investigation.

Additionally, the present economic evaluation is limited to initial investment and simple payback, without accounting for maintenance costs or full life-cycle impacts. While electrochemical polishing of aluminum is a robust, low-maintenance process with no recurring costs under typical window operating conditions, long-term durability (e.g., resistance to condensation, oxidation, or mechanical abrasion) remains unverified. Future work should include a comprehensive life-cycle cost analysis (LCCA) and accelerated aging tests to quantify these factors.

5. Conclusions

This study systematically investigated the impact of cavity inner-surface low-emissivity treatment on the thermal performance of broken-bridge aluminum alloy window frames and complete assemblies through theoretical analysis and simulations. Using a typical 75-series casement window and representative cities across China's five thermal climate zones, the energy-saving potential and regional applicability of the technology were rigorously evaluated. The key findings are summarized as follows:

(1) Reducing cavity inner-surface emissivity significantly lowers both frame and whole-window U-values. Compared to the baseline (Case B), full-cavity ultra-low-emissivity treatment (Case D-1) achieves frame U-value reductions of 12.39–30.38% and whole-window reductions of 2.72–9.69%.

(2) Comprehensive treatment of all cavity surfaces maximizes performance, yielding an average frame U-value reduction of 0.29 $W/(m^2 \cdot K)$ compared to insulating-cavity-only treatment, underscoring the critical role of radiative suppression across all internal boundaries.

(3) Although the low-emissivity frame does not fully match the insulation level of polyurethane foam-filled frames (Case A), the whole-window U-value of Case D-1 is lower due to reduced thermal bridging at the frame–glazing interface, where linear thermal transmittance is minimized.

(4) The technology is highly effective in heating-dominated climates (e.g., Harbin, Beijing), delivering up to 2.26% annual energy savings (8.99 $MJ/m^2 \cdot yr$). However, it increases cooling loads in mild or cooling-dominated regions (Guangzhou, Kunming) and offers negligible benefit in balanced climates (Shanghai).

(5) At an incremental cost of 62.5 CNY per window (6.6–7.4% increase over baseline), full-cavity treatment yields a static payback period of 4.1 years in Harbin and 17.9 years in Beijing for a six-window office room. This cost-effectiveness, combined with minimal structural intervention, positions the technology as a promising retrofit solution for existing buildings in northern China.

In conclusion, low-emissivity cavity treatment offers a low-cost, high-impact strategy for enhancing window thermal performance, particularly in cold and severe cold climates. However, its deployment in transitional or cooling-dominated regions requires careful case-by-case assessment to account for interactions with passive cooling strategies, shading, ventilation, and thermal mass. Future studies incorporating whole-building dynamics and real operational data are recommended to refine these contextual guidelines.

Author Contributions: Conceptualization, M.X. and J.K.; methodology, M.X.; investigation, M.X.; writing—original draft preparation, M.X.; writing—review and editing, M.X. and J.K.; visualization, M.X. and J.K.; supervision, J.K. and S.K.; funding acquisition, M.X. and J.K. All authors have read and agreed to the published version of the manuscript.

Funding: This research received no external funding.

Institutional Review Board Statement: Not applicable.

Informed Consent Statement: Not applicable.

Data Availability Statement: The original contributions presented in this study are included in the article. Further inquiries can be directed to the corresponding author.

Conflicts of Interest: Author Maohua Xiong was employed by the China Construction Eighth Engineering Division Corp., Ltd. The remaining authors declare that the research was conducted in the absence of any commercial or financial relationships that could be construed as a potential conflict of interest.

Appendix A

Energy consumption intensity of different directions in five cities is shown in Table A1.

Table A1. Energy consumption intensity of different directions in five cities.

Scenario	Axis to North (°)	Harbin (MJ/m²·yr)	Beijing (MJ/m²·yr)	Shanghai (MJ/m²·yr)	Guangzhou (MJ/m²·yr)	Kunming (MJ/m²·yr)
A	0	337.97	197.7	228.97	322.73	246.64
	90	424.46	257.68	255.89	331.42	266.4
	180	397.63	211.43	196.33	269.72	166.38
	270	410.16	231.19	229.33	300.44	194.19
B	0	341.86	196.74	227.58	320.81	242.96
	90	428.44	258.26	255.07	329.43	262.68
	180	402.4	214.22	196.2	268.23	164.15
	270	414.4	232.21	228.74	298.74	191.59
C-1	0	334.65	198.47	230.02	324.13	249.37
	90	421.62	257.27	256.56	332.85	269.16
	180	394.14	209.3	196.42	270.83	168.06
	270	407.14	230.52	229.78	301.74	196.19
C-2	0	339.57	197.28	228.39	321.93	245.06
	90	426.1	257.87	255.55	330.63	264.81
	180	399.65	213.05	196.26	269.09	165.43
	270	411.97	231.61	229.05	299.73	193.08
D-1	0	333.15	198.88	230.58	324.92	250.83
	90	420.19	257.1	256.92	333.62	270.61
	180	392.23	208.6	196.49	271.44	168.95
	270	405.6	230.2	230.01	302.47	197.21
D-2	0	339.29	197.34	228.44	322.04	245.29
	90	425.89	257.87	255.6	330.73	265.05
	180	399.36	212.93	196.26	269.18	165.56
	270	411.67	231.56	229.1	299.84	193.23

References

1. Dwyer, S.; Teske, S. *Renewables 2019 Global Status Report*; REN21: Paris, France, 2019.
2. Jagarajan, R.; Asmoni, M.N.A.M.; Mohammed, A.H.; Jaafar, M.N.; Mei, J.L.Y.; Baba, M. Green retrofitting–A review of current status, implementations and challenges. *Renew. Sustain. Energy Rev.* **2017**, *67*, 1360–1368. [CrossRef]
3. Casini, M. Active dynamic windows for buildings: A review. *Renew. Energy* **2018**, *119*, 923–934. [CrossRef]
4. Hui, Y.; Chuang, Y.; Xingzhong, G.U.O.; Tinggui, Y. Research status of building energy-saving doors and Windows and technology. *New Build. Mater.* **2012**, *39*, 84–89. [CrossRef]
5. Hong, L.; Zhou, N.; Feng, W.; Khanna, N.; Fridley, D.; Zhao, Y.; Sandholt, K. Building stock dynamics and its impacts on materials and energy demand in China. *Energy Policy* **2016**, *94*, 47–55. [CrossRef]
6. Ni, H. *Suggestions on Increasing Subsidies for Energy-Saving Window and Door Renovations to Stimulate New Consumer Demands*; Hebei Aorun Shunda Window Industry Co., Ltd.: Gaobeidian, China, 2025.
7. Hu, N.; Jie, Y. Low-Standard Doors and Windows Have Become an Invisible "Black Hole". The Industry Calls for Raising Industry Standards. Available online: http://www1.xinhuanet.com/fortune/20240222/6032ae84f415448f9c2f74a7a6d6448a/c.html (accessed on 22 February 2024).
8. Song, Z.; Li, J.-l.; Li, Y. Energy-Saving Performance of Nano Insulated Coating Glass. *Build. Energy Effic.* **2014**, *42*, 38–41. [CrossRef]
9. Garlisi, C.; Trepci, E.; Li, X.; Al Sakkaf, R.; Al-Ali, K.; Nogueira, R.P.; Zheng, L.; Azar, E.; Palmisano, G. Multilayer thin film structures for multifunctional glass: Self-cleaning, antireflective and energy-saving properties. *Appl. Energy* **2020**, *264*, 114697. [CrossRef]
10. Liao, Q.; Guan, Y.; Wang, Q. Research of window's discharge coefficient in the natural ventilation room. *Appl. Mech. Mater.* **2014**, *525*, 420–426. [CrossRef]

11. Lei, Q.; Wang, L.; Xie, H.; Yu, W. Active-passive dual-control smart window with thermochromic synergistic fluidic glass for building energy efficiency. *Build. Environ.* **2022**, *222*, 109407. [CrossRef]
12. Chang, J.Y.; Kuan, Y.D.; Lan, C.C.; Li, H.J.; Hsu, Y.K.; Chen, C.Y.; Shen, E.T.; Lin, K.Y. Discussion of the Energy-Saving Benefits of Heat Insulating Coating for Building Windows. In Proceedings of the International Conference on Electronic, Information and Computer Engineering (ICEICE), Hong Kong, China, 26–27 April 2016.
13. Zajas, J.; Heiselberg, P. Parametric study and multi objective optimization of window frame geometry. *Build. Simul.* **2014**, *7*, 579–593. [CrossRef]
14. Appelfeld, D.; Hansen, C.S.; Svendsen, S. Development of a slim window frame made of glass fibre reinforced polyester. *Energy Build.* **2010**, *42*, 1918–1925. [CrossRef]
15. Cardinale, N.; Rospi, G.; Cardinale, T. Numerical and experimental thermal analysis for the improvement of various types of windows frames and rolling-shutter boxes. *Int. J. Energy Environ. Eng.* **2015**, *6*, 101–110. [CrossRef]
16. Su, X.P.; Sun, W.D. The energy-saving design and construction study on exterior windows in the building. *Adv. Mater. Res.* **2014**, *1004–1005*, 1556–1559. [CrossRef]
17. Huang, H.; Wang, H.; Hu, Y.-J.; Li, C.; Wang, X. The development trends of existing building energy conservation and emission reduction—A comprehensive review. *Energy Rep.* **2022**, *8*, 13170–13188. [CrossRef]
18. Paulos, J.; Berardi, U. Optimizing the thermal performance of window frames through aerogel-enhancements. *Appl. Energy* **2020**, *266*, 114776. [CrossRef]
19. Lechowska, A.A.; Schnotale, J.A.; Baldinelli, G. Window frame thermal transmittance improvements without frame geometry variations: An experimentally validated CFD analysis. *Energy Build.* **2017**, *145*, 188–199. [CrossRef]
20. *EN ISO 10077-2*; Thermal Performance of Windows, Doors and Shutters—Calculation of Thermal Transmittance. Part 2: Numerical Method for Frames. NSAI Standard: Dublin, Ireland, 2012.
21. Asdrubali, F.; Baldinelli, G.; Bianchi, F. Influence of cavities geometric and emissivity properties on the overall thermal performance of aluminum frames for windows. *Energy Build.* **2013**, *60*, 298–309. [CrossRef]
22. Rosencrantz, T.; Bulow-Hube, H.; Karlsson, B.; Roos, A. Increased solar energy and daylight utilisation using anti-reflective coatings in energy-efficient windows. *Sol. Energy Mater. Sol. Cells* **2005**, *89*, 249–260. [CrossRef]
23. Mitchell, R.; Kohler, C.; Arasteh, D.; Carmody, J.; Huizenga, C.; Curcija, D. *THERM 5/WINDOW 5 NFRC Simulation Manual*; Technical Report; Lawrence Berkeley National Laboratory: Berkeley, CA, USA, 2003.
24. Van Den Bergh, S.; Hart, R.; Jelle, B.P.; Gustavsen, A. Window spacers and edge seals in insulating glass units: A state-of-the-art review and future perspectives. *Energy Build.* **2013**, *58*, 263–280. [CrossRef]
25. *GB/T30591-2014*; Requirements for the Coordination of Dimensions of Building Door and Window Openings. China Standards Press: Beijing, China, 2014.
26. *GB/T8478-2020*; Aluminum Doors and Windows. China Standards Press: Beijing, China, 2020.
27. Zhao, J.; Lu, Y.; Yang, L. The influence of insulation materials on the thermal performance of passive aluminum alloy windows. *Constr. Sci. Technol.* **2019**, *9*, 26–33.
28. Touloukian, Y. Thermal radiative properties of non-metallic solids, Thermophysical properties of matter. *TPRC Data Ser.* **1972**, *8*, 383.
29. Wen, C.-D.; Mudawar, I. Emissivity characteristics of polished aluminum alloy surfaces and assessment of multispectral radiation thermometry (MRT) emissivity models. *Int. J. Heat Mass Transf.* **2005**, *48*, 1316–1329. [CrossRef]
30. Brusov, A.; Orr, G.; Azoulay, M.; Golan, G. Electropolishing of single crystal and polycrystalline aluminum to achieve high quality optical and mechanical surfaces. *Bulg. Chem. Commun.* **2020**, *52*, 5–11. [CrossRef]
31. Adelkhani, H.; Nasoodi, S.; Jafari, A. A study of the morphology and optical properties of electropolished aluminum in the Vis-IR region. *Int. J. Electrochem. Sci.* **2009**, *4*, 238–246. [CrossRef]
32. *JGJ/T 151-2008*; Calculation Specification for Thermal Performance of Windows, Doors and Glass Curtain-Walls. China Architecture & Building Press: Beijing, China, 2008.
33. *GBT8484-2020*; Testing Methods for the Thermal Insulation Performance for Building Exterior Doors and Windows. China Standards Press: Beijing, Chins, 2020.
34. Zhou, X.Q.; Zhu, Y.Y.; Peng, H.W.; Zeng, Z.W.; Huang, Y.; Li, L. Energy efficiency optimization for building envelopes on a green campus in Guangzhou. In Proceedings of the 4th Asia Conference of International-Building-Performance-Simulation-Association (ASIM), Hong Kong, China, 3–5 December 2018.
35. Imbert, P.; Larsen, O.K.; Johra, H. Study of thermochromic glass performance in the Danish climate and visual comfort perspectives. In Proceedings of the International Conference on Climate Resilient Cities—Energy Efficiency and Renewables in the Digital Era (CISBAT), Ecole Polytechnique Fed Lausanne, Solar Energy & Building Phys Lab, Lausanne, Switzerland, 4–6 September 2019.
36. Liu, M.; Heiselberg, P.K.; Antonov, Y.I.; Mikkelsen, F.S. Parametric analysis on the heat transfer, daylight and thermal comfort for a sustainable roof window with triple glazing and external shutter. *Energy Build.* **2019**, *183*, 209–221. [CrossRef]

37. *GB 50189-2015*; Design Standard for Energy Efficiency of Public Buildings. Standardization Administration of the People's Republic of China: Beijing, China, 2015.
38. Zhang, Q. Development of the typical meteorological database for Chinese locations. *Energy Build.* **2006**, *38*, 1320–1326. [CrossRef]
39. Mohammad, A.E.K.; Wang, D. Electrochemical mechanical polishing technology: Recent developments and future research and industrial needs. *Int. J. Adv. Manuf. Technol.* **2016**, *86*, 1909–1924. [CrossRef]
40. Wang, J.; Qin, J.; Shao, S. *In-Depth Analysis of Aluminum in the Industrial Metals Industry: Constrained Capacity, Favorable Pattern, Embracing the Era of High-Profit Electrolytic Aluminum*; Citic China Securities: Beijing, China, 2025.
41. Stegnar, G. Strategic Prioritization of Residential Buildings for Equitable and Sustainable Renovation. *Sustainability* **2025**, *17*, 2203. [CrossRef]
42. Pacheco-Torgal, F.; Granqvist, C.-G.; Jelle, B.P.; Vanoli, G.P.; Bianco, N.; Kurnitski, J. *Cost-Effective Energy Efficient Building Retrofitting: Materials, Technologies, Optimization and Case Studies*; Woodhead publishing: Cambridge, UK, 2017.
43. *ASTM C1371-15*; Standard Test Method for Determination of Emittance of Materials Near Room Temperature Using Portable Emissometers. ASTM International: West Conshohocken, PA, USA, 2015.

Disclaimer/Publisher's Note: The statements, opinions and data contained in all publications are solely those of the individual author(s) and contributor(s) and not of MDPI and/or the editor(s). MDPI and/or the editor(s) disclaim responsibility for any injury to people or property resulting from any ideas, methods, instructions or products referred to in the content.